Shock Waves (1993) 3:95–104

Shock Waves

Propagation of blast waves with exponential heat release and internal heat conduction and thermal radiation

W. Gretler and P. Wehle

Institute of Fluid Mechanics and Gas Dynamics, Technical University of Graz, Inffeldgasse 25, 8010 Graz, Austria

Received March 23, 1992; accepted August 25, 1992

Abstract. The problem of reactive blast waves in a combustible gas mixture, where the heat release at the detonation front decays exponentially with the distance from the center, is analyzed. The central theme of the paper is on the propagation of reactive blast into a uniform, quiescent, counterpressure atmosphere of a perfect gas with constant specific heats. The limiting cases of Chapman-Jouguet detonation waves are considered in the phenomenon of point explosion. In order to deal with this problem, the governing equations including thermal radiation and heat conduction were solved by the method of characteristics using a problem-specific grid and a series expansion as start solution. Numerical results for the distribution of the gas-dynamic parameters inside the flow field are shown and discussed.

Key words: Chapman-Jouguet detonation, Explosion, Heat conduction, Numerical results, Reactive blast waves, Thermal radiation

1. Introduction

Detonations can be initiated in unconfined fuel-air clouds by blast waves of sufficient energy. The pressure and velocity induced behind such detonations can result in extensive damage. In the present paper, the propagation of reactive blast waves through a medium with a spatially nonuniform fuel concentration is analyzed. The blast wave consists of a single wave front in which combustion is completed and the energy instantaneously released. The chemical heat release Q is determined by the chemical composition and the thermodynamic states of the reactants and products. In this analysis, Q is assumed to depend only on the initial chemical composition, which varies with the distance from the explosion center.

The detonation is restricted to a zone behind the wave front where complex physico-chemical phenomena occur. For simplicity, these phenomena are neglected in the applied single surface model of a detonation wave (Fig. 1). The reaction front and the shock front have the same location and the change of the chemical energy with the distance from the explosion center is characterized by

$$Q = Q_0 \exp\left(-\beta \frac{r_n}{r_0}\right), \tag{1}$$

where Q_0, r_0, and β are constants given a priori.

Ohyagi and Ohsawa (1983) solved the blast wave equations for the described simplified model but their quasi-similar technique based on the work of Oshima (1960) only gives an approximate solution. The purpose of the present paper is to find a more accurate solution by using the special method of characteristics for non-adiabatic explosion problems developed by Wehle and Gretler (1991). The traditional method of characteristics associated with a problem-specific grid, as already shown in previous papers, is very accurate in the smooth parts of the flow field and resolves discontinuities such as shock and detonation fronts with zero width. In recent times other numerical schemes became meaningful, including those for hyperbolic systems with two independent variables as in the problem at hand. However, modern schemes are developed for specific purposes only and most of them have the disadvantage of smearing the shock, or are inclined to produce spurious oscillations at discontinuities. In the present paper the physically unrealistic features of infinite temperature and zero density at the center of symmetry for all times are also avoided by taking convective and radiative heat transfer effects into account.

2. Basic equations

The basic conservation equations of mass, momentum and energy for the one-dimensional unsteady flow of a perfect gas, with heat conduction and radiation taken into account, may in Eulerian coordinates be expressed as

$$\frac{\partial \rho}{\partial t} + u\frac{\partial \rho}{\partial r} + \rho\frac{\partial u}{\partial r} + j\frac{\rho u}{r} = 0, \tag{2}$$

$$\frac{\partial u}{\partial t} + u\frac{\partial u}{\partial r} + \frac{1}{\rho}\frac{\partial p}{\partial r} = 0, \tag{3}$$

Correspondence to: W. Gretler

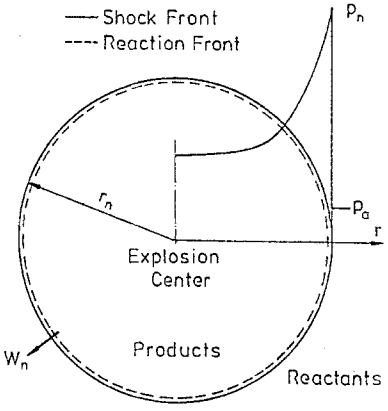

Fig. 1. Scheme of a gas flow in the model of a single front

$$\frac{\partial e}{\partial t}+u\frac{\partial e}{\partial r}+p\left[\frac{\partial}{\partial t}\left(\frac{1}{\rho}\right)+u\frac{\partial}{\partial r}\left(\frac{1}{\rho}\right)\right] = -\frac{1}{\rho r^j}\frac{\partial}{\partial r}\left(r^j q\right). \tag{4}$$

Here r and t are independent space and time coordinates and ρ, u, p, e, and q express the density, flow velocity, pressure, specific internal energy and the heat flux, respectively. κ and j denote the specific heat ratio and a geometric factor which takes the value of 0 in the planar, 1 in the cylindrical and 2 in the spherical case.

As in the usual blast wave problem, the gas behaviour is expressed in terms of two thermodynamic properties, namely the specific internal energy

$$e=\frac{1}{\kappa-1}\frac{p}{\rho} \tag{5}$$

and the speed of sound

$$a^2=\kappa\frac{p}{\rho}. \tag{6}$$

The total heat flux q, which appears in the energy equation, may be decomposed as

$$q=q_C+q_R. \tag{7}$$

According to Fourier's law of heat conduction

$$q_C=-K\frac{\partial T}{\partial r}, \tag{8}$$

where K is the thermal conductivity of the gas and T is the absolute temperature. Assuming local thermodynamic equilibrium and using the radiative diffusion model for an optically thick grey gas (Pomraning 1973), the term q_R, which represents radiative heat flux, may be obtained from the differential approximation of the radiation-transport equation in the diffusion limit

$$q_R=-\frac{16}{3}\frac{\sigma T^3}{\alpha_R}\frac{\partial T}{\partial r}, \tag{9}$$

where σ is the Stefan Boltzmann constant and α_R is the Rosseland mean absorption coefficient defined by Pomraning (1973). The thermal conductivity K and the absorption coefficient α_R are assumed to vary as

$$K=K_a\left(\frac{T}{T_a}\right)^{\beta_C} \text{ and } \alpha_R=\alpha_{R_a}\left(\frac{T}{T_a}\right)^{\beta_R}, \tag{10}$$

respectively, where the subscript a denotes atmospheric conditions. In order to obtain a self-similar solution the temperature exponents in the above equations should satisfy the similarity requirements and are given by (see e.g. Abdel-Raouf and Gretler 1991)

$$\beta_C=\frac{1}{2}-\frac{1}{j+1} \text{ and } \beta_R=\frac{5}{2}+\frac{1}{j+1}. \tag{11}$$

To obtain a solution valid regardless of the state of the surroundings, it is convenient to introduce a non-dimensional representation for the independent variables

$$r^*=\frac{r}{r_0},\ t^*=\frac{a_a t}{r_0}, \tag{12}$$

and for the corresponding dependent variables

$$u^*=\frac{u}{a_a},\ a^*=\frac{a}{a_a},\ p^*=\frac{p}{p_a},\ q^*=\frac{q}{\rho_a a_a^3}, \text{ and } Q^*=\frac{Q}{a_a^2} \tag{13}$$

which describe the structure of the flow field. r_0 is the characteristic length of the field defined by Oppenheim et al. (1971)

$$r_0=\left(\frac{E_i}{p_a}\right)^{\frac{1}{j+1}}. \tag{14}$$

If one finally introduces non-dimensional heat parameters as

$$\Gamma_C=\frac{K_a T_a}{\rho_a a_a^3 r_0} \text{ and } \Gamma_R=\frac{\sigma T_a^4}{\rho_a a_a^3 r_0 \alpha_{R_a}}, \tag{15}$$

one may summarize (8), (9), and (7) together with the application of the power-laws (10) and the exponents (11) in a single equation for representation of the non-dimensional heat flux:

$$q^*=q_C^*+q_R^*=-\Gamma T^{*\beta_C}\frac{\partial T^*}{\partial r^*} \text{ with } \Gamma=\Gamma_C+\frac{16}{3}\Gamma_R. \tag{16}$$

The necessary boundary conditions are given by the conservation equations across the reaction front and symmetry conditions. With terms for total heat flux and chemical heat release included, the conditions behind the reaction front are

$$u_n^*=\frac{1}{\kappa+1}\left\{\left(W_n^*-\frac{1}{W_n^*}\right)+\left[\left(W_n^*-\frac{1}{W_n^*}\right)^2-2(\kappa-1)(\kappa+1)\left(\frac{q_n^*}{W_n^*}+Q^*\right)\right]^{\frac{1}{2}}\right\}, \tag{17}$$

$$a_n^*=\left[\left(1+\kappa u_n^* W_n^*\right)\left(1-\frac{u_n^*}{W_n^*}\right)\right]^{\frac{1}{2}}, \tag{18}$$

$$p_n^* = 1 + \kappa u_n^* W_n^*, \tag{19}$$

where the non-dimensional velocity of the reaction front W_n^* is defined by

$$W_n^* = \frac{\mathrm{d}r_n^*}{\mathrm{d}t^*}, \tag{20}$$

and n denotes the state immediately behind the reaction front. In the detonation center the symmetry conditions are

$$u^*(0, t^*) = 0 \text{ and } q^*(0, t^*) = 0. \tag{21}$$

The results of our numerical computations were checked by applying the laws of conservation of mass and energy in the following form:

$$\frac{M_j}{n_j} = \int_0^{r_n} \rho r^j \mathrm{d}r = \frac{\rho_a r_n^{j+1}}{j+1}, \tag{22}$$

$$\frac{E_j}{n_j} = \int_0^{r_n} \left(e + \frac{u^2}{2}\right) \rho r^j \mathrm{d}r = p_a r_0^{j+1} + \frac{\rho_a e_a r_n^{j+1}}{j+1} + \frac{Q \rho_a r_n^{j+1}}{j+1} + \frac{\beta \rho_a}{(j+1) r_0} \int_0^{r_n} Q r_n^{j+1} \mathrm{d}r_n, \tag{23}$$

where M_j is the total mass content inside the flow field, E_j the total energy of the blast wave and $n_j = 2\pi j + \frac{1}{2}(j-1)(j-2)$ a geometrical factor.

3. Perturbation solution

In order to perform the integration of the system of equations above, initial conditions are required besides the boundary conditions. A coordinate expansion for the limiting cases $\beta = 0$ and $\beta = \infty$ (see (1)) based on the reciprocal square of the front Mach number can be employed to obtain solutions for the initial stages of blast waves with non-zero counterpressure as discussed in our previous paper (Kailbauer and Gretler 1991). In the present detonation case the heat release is taken into account to first order, so that the basic similarity solution is unaltered in the conservation equations at the reaction front. A brief presentation of this modified perturbation solution, which also serves as an initial condition for the integration in the transition case $0 < \beta < \infty$, now follows.

The time and space coordinates are replaced by non-dimensional new independent variables, the similarity variable $x = r/r_n(t)$ and the non-dimensional front radius $\xi = r_n(t)/r_0$. With ξ and the reciprocal of the square of the reaction front Mach number $y = a_a^2/W_n^2(t)$ a relation for the decay parameter can be formed:

$$\lambda = -2\frac{\ddot{r}_n}{\dot{r}_n^2/r_n} = \frac{\mathrm{d}\ln y}{\mathrm{d}\ln \xi}. \tag{24}$$

The system of differential equations (2)–(4) expressed in a non-dimensional form is

$$\lambda y \frac{\partial h}{\partial y} + (f - x)\frac{\partial h}{\partial x} + h\left(\frac{\partial f}{\partial x} + j\frac{f}{x}\right) = 0, \tag{25}$$

$$\lambda y \frac{\partial f}{\partial y} + (f - x)\frac{\partial f}{\partial x} + \frac{1}{h}\frac{\partial g}{\partial x} - \frac{\lambda}{2} f = 0, \tag{26}$$

$$\lambda y \frac{\partial g}{\partial y} + (f - x)\frac{\partial g}{\partial x} - \frac{\kappa g}{h}\left[(f - x)\frac{\partial h}{\partial x} + \lambda y \frac{\partial h}{\partial y}\right] - \lambda g = -(\kappa - 1)\left(\frac{j\tilde{q}}{x} + \frac{\partial \tilde{q}}{\partial x}\right). \tag{27}$$

Here the dependent variables are defined as

$$f = u^* \sqrt{y},\ g = \frac{p^*}{\kappa} y,\ h = \frac{\rho}{\rho_a} = \rho^*,\ \tilde{q} = q^* y^{\frac{3}{2}} \tag{28}$$

and the expression for the internal heat flux is given by

$$\tilde{q} = \tilde{q}_C + \tilde{q}_R = -\left[\Gamma_C \frac{y^{\frac{1}{2}-\beta_C}}{\xi}\left(\frac{\kappa g}{h}\right)^{\beta_C} + \frac{16}{3}\Gamma_R \frac{y^{\beta_R - \frac{5}{2}}}{\xi}\left(\frac{\kappa g}{h}\right)^{3-\beta_R}\right]\frac{\partial}{\partial x}\left(\frac{\kappa g}{h}\right). \tag{29}$$

The boundary conditions (17)–(21) and the integral relations (22) and (23) may now be represented in the corresponding non-dimensional form:

$$f_i = 0,\ \tilde{q}_i = 0, \tag{30}$$

$$h_n = \frac{1}{1 - f_n},\ g_n = f_n + \frac{y}{\kappa}, \tag{31}$$

$$f_n = \frac{1}{\kappa + 1}\left\{(1 - y) + \left[(1 - y)^2 - 2(\kappa^2 - 1)(\tilde{q}_n + Q^* y)\right]^{\frac{1}{2}}\right\}, \tag{32}$$

$$I = \frac{M_j}{n_j \rho_a r_n^{j+1}} = \int_0^1 h x^j \mathrm{d}x = \frac{1}{j+1}, \tag{33}$$

$$J = \frac{E_j}{n_j \rho_a r_n^{j+1} W_n^2} = \int_0^1 \left(\frac{g}{\kappa - 1} + \frac{1}{2} h f^2\right) x^j \mathrm{d}x = \frac{y}{\kappa}\left(\xi^{-(j+1)} + \frac{1}{(j+1)(\kappa - 1)} + \frac{\kappa Q^*}{j+1}\right). \tag{34}$$

Series expansions in y give

$$f(x, y) = f_0(x) + f_1(x) y + O(y^2), \tag{35}$$

$$g(x, y) = g_0(x) + g_1(x) y + O(y^2), \tag{36}$$

$$h(x, y) = h_0(x) + h_1(x) y + O(y^2), \tag{37}$$

$$\tilde{q}(x, y) = \tilde{q}_0(x) + \tilde{q}_1(x) y + O(y^2), \tag{38}$$

$$\lambda(y) = \lambda_0 + \lambda_1 y + O(y^2),\ \xi^{j+1} = \xi_1 y + \xi_2 y^2 + O(y^3), \tag{39}$$

$$I(y) = I_0 + I_1 y + O(y^2),\ J(y) = J_0 + J_1 y + O(y^2). \tag{40}$$

Since the energy released by chemical reactions is negligible compared with the blast wave energy E_0, the Q_0^*-term enters as the counterpressure only into the first order term. Solutions can now be found successively starting from the similarity (zeroth-order) solution. Substituting (35)–(40) into the non-dimensional governing equations (25)–(27), the boundary conditions (30)–(32) and the integral relations (33)

and (34) and then equating the coefficients of terms with the same power of y gives for the y^0 terms

$$(f_0 - x)h_0' + h_0 f_0' = -\frac{j}{x} f_0 h_0, \tag{41}$$

$$(f_0 - x)f_0' h_0 + g_0' = \frac{\lambda_0}{2} f_0 h_0, \tag{42}$$

$$\begin{aligned}(f_0 - x)g_0' + \kappa g_0 f_0' + (\kappa - 1)\tilde{q}_0' \\ = -\frac{\kappa j}{x} g_0 f_0 + \lambda_0 g_0 - (\kappa - 1)\frac{j\tilde{q}_0}{x},\end{aligned} \tag{43}$$

$$\tilde{q}_0 = -(\kappa J_0)^{\frac{1}{j+1}} \Gamma \left(\frac{\kappa g_0}{h_0}\right)^{\beta_C} \left(\frac{\kappa g_0}{h_0}\right)', \tag{44}$$

where in (44) the relation $\xi_1 = 1/\kappa J_0$ has been used. The boundary conditions are

$$f_{0i} = 0, \quad \tilde{q}_{0i} = 0, \tag{45}$$

$$\begin{cases} g_{0n} = f_{0n}, \quad h_{0n} = \dfrac{1}{1 - f_{0n}}, \\ \tilde{q}_{0n} = \dfrac{f_{0n}}{\kappa - 1} - \dfrac{\kappa + 1}{2(\kappa - 1)} f_{0n}^2, \end{cases} \tag{46}$$

$$\begin{cases} I_0 = \displaystyle\int_0^1 h_0 x^j \mathrm{d}x = \frac{1}{j+1}, \\ J_0 = \displaystyle\int_0^1 \left(\frac{1}{2} h_0 f_0^2 + \frac{g_0}{\kappa - 1}\right) x^j \mathrm{d}x, \end{cases} \tag{47}$$

where the dash denotes the differentiation with respect to x. From the coefficient of y^1 terms one gets

$$\begin{aligned}h_0 f_1' - (x - f_0)h_1' \\ = -\left(h_0' + \frac{h_0 j}{x}\right) f_1 - \left(f_0' + \frac{j f_0}{x} + \lambda_0\right) h_1,\end{aligned} \tag{48}$$

$$\begin{aligned}h_0(f_0 - x)f_1' + g_1' = -h_0 f_1 \left(f_0' + \frac{\lambda_0}{2}\right) \\ + \left[\frac{\lambda_0 f_0}{2} + (x - f_0)f_0'\right] h_1 + \frac{\lambda_1 f_0 h_0}{2},\end{aligned} \tag{49}$$

$$\begin{aligned}\kappa g_0 f_1' - (x - f_0)g_1' + (\kappa - 1)\tilde{q}_1' \\ = -\left(g_0' + \frac{\kappa j g_0}{x}\right) f_1 - \kappa g_1 \left(f_0' + \frac{j f_0}{x}\right) \\ + \lambda_1 g_0 - (\kappa - 1)\frac{\tilde{q}_1 j}{x},\end{aligned} \tag{50}$$

$$\begin{aligned}\tilde{q}_1 = \tilde{q}_0 \left[\left(\frac{g_1}{g_0} - \frac{h_1}{h_0}\right)(\beta_C + 1)\right. \\ \left. + \left(\frac{g_0'}{g_0} - \frac{h_0'}{h_0}\right)^{-1} \left(\frac{g_1}{g_0} - \frac{h_1}{h_0}\right)' + \frac{\lambda_1}{\lambda_0^2}\right].\end{aligned} \tag{51}$$

From (34) follows

$$\xi_2 = \xi_1^2 \kappa \left(\frac{1}{\kappa(j+1)(\kappa - 1)} - J_1 + \frac{Q_0^*}{j+1}\right), \tag{52}$$

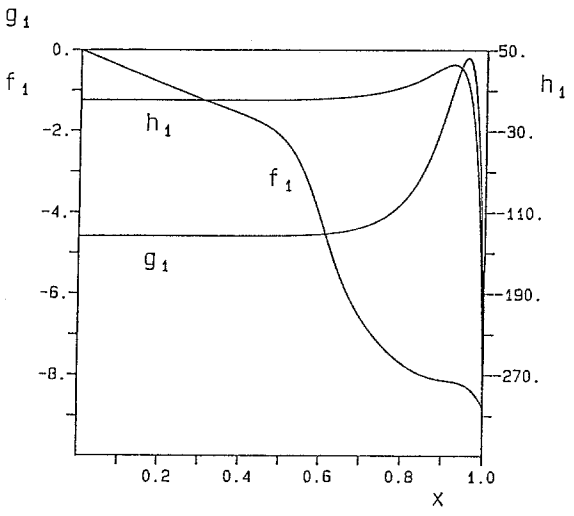

Fig. 2. Coefficients of the first order solutions of f, g, and h versus the field coordinate x

which with the relation for λ_1 gives

$$\lambda_1 = \frac{1}{J_0}\left[(j+1)J_1 - \frac{1}{\kappa(\kappa - 1)} - Q_0^*\right]. \tag{53}$$

The boundary conditions are

$$f_{1i} = 0, \quad \tilde{q}_{1i} = 0, \tag{54}$$

$$g_{1n} = f_{1n} + \frac{1}{\kappa}, \quad h_{1n} = \frac{f_{1n}}{(1 - f_{0n})^2}, \tag{55}$$

$$\tilde{q}_{1n} = \frac{1}{\kappa - 1}\left[f_{1n} - f_{0n} - (\kappa + 1) f_{0n} f_{1n}\right], \tag{56}$$

while the coefficients of the integral relations may be written as

$$\begin{cases} I_1 = \displaystyle\int_0^1 h_1 x^j \mathrm{d}x = 0, \\ J_1 = \displaystyle\int_0^1 \left(\frac{h_1 f_0^2}{2} + h_0 f_1 f_0 + \frac{g_1}{\kappa - 1}\right) x^j \mathrm{d}x. \end{cases} \tag{57}$$

While the zeroth-order solution can be taken from Kailbauer and Gretler (1991), in the case of the first-order solution the set of linear nonhomogeneous differential equations (48)–(51) and the boundary conditions (54)–(56) specify a two-point boundary-value problem. To find the correct λ_1 value from (53), an iteration method similar to that described in the afore-mentioned paper is used. The reduced variables for velocity, pressure and density as functions of the similarity variable x are presented in Fig. 2, where the corresponding $\lambda_1 = -88.672$.

4. Chapman-Jouguet detonation

In contrast to the classical works of Jouguet (1917), Zel'dovich (1942) and Taylor (1950), where a Chapman-Jouguet CJ-wave is assumed to be initiated instantaneously

at $r = 0$ ($y = 0$) and propagates with a constant front velocity, the flow in the initial stage of the explosion will not follow the CJ-rule (cf., for example, Korobeinikov 1969). In the initial stage of the process $u_n + a_n > W_n$, i.e. where the right-running expansion waves meet the shock, an overcompressed detonation occurs. During the propagation of the shock wave the slope of right-running characteristics at the wave front ($(\mathrm{d}r/\mathrm{d}t)|_\eta = u_n + a_n$) decreases, and the passage to the regime of CJ-detonation is possible (Fig. 13).

Depending on the heat parameter β (Eq. (1)) when the limiting case of the CJ-detonation is obtained at a certain moment ($y > 0$) and a certain distance from the center ($r > 0$), the expression in the root of (17) vanishes, and this leads to the following equations:

$$\tilde{q}_n + Q^* y_{CJ} = \frac{(1 - y_{CJ})^2}{2(\kappa^2 - 1)}, \tag{58}$$

$$f_n = \frac{1 - y_{CJ}}{\kappa + 1}, \quad h_n = \frac{1}{1 - f_n}, \quad g_n = f_n + \frac{y_{CJ}}{\kappa}. \tag{59}$$

It is easy to see from (59) that for $y = y_{CJ} > 0$

$$f_n + \sqrt{\frac{\kappa g_n}{h_n}} = 1 \tag{60}$$

and

$$u_n + a_n = W_n. \tag{61}$$

The above equation confirms the CJ-condition that the velocity of the wave relative to the heated fluid is identical with the local sound speed. Equation (58) differentiated with respect to ξ and the definition of λ, given by (24), expresses the decay parameter in the following functional form:

$$\lambda_{CJ} = \left(\frac{\mathrm{d}\ln y}{\mathrm{d}\ln \xi}\right)_{CJ} = \frac{(\kappa^2 - 1)\left(\beta Q^* - \frac{\mathrm{d}q_n^*}{\mathrm{d}\xi}\sqrt{y_{CJ}}\right)\xi}{1 - y_{CJ} + (\kappa^2 - 1)\left(Q^* + \frac{3}{2}q_n^*\sqrt{y_{CJ}}\right)}. \tag{62}$$

Taking into consideration that

$$\left(\frac{\mathrm{d}q_n^*}{\mathrm{d}\xi}\right)_{CJ} \approx q_{nCJ}^* \approx 0, \tag{63}$$

one can obtain

$$\lambda_{CJ} = \frac{(\kappa^2 - 1)(1 - y_{CJ})\beta\xi}{1 + y_{CJ}}. \tag{64}$$

From this expression one may conclude that only the case $\beta = 0, \xi > 0$ represents the limiting case $\lambda_{CJ} = 0$ of the well-known solution for constant-velocity CJ-detonation. This is the classical case in which a constant propagation speed associated with a uniform undisturbed medium leads to a homentropic flow field within the whole blast wave as a consequence of a constant entropy rise across the wave front.

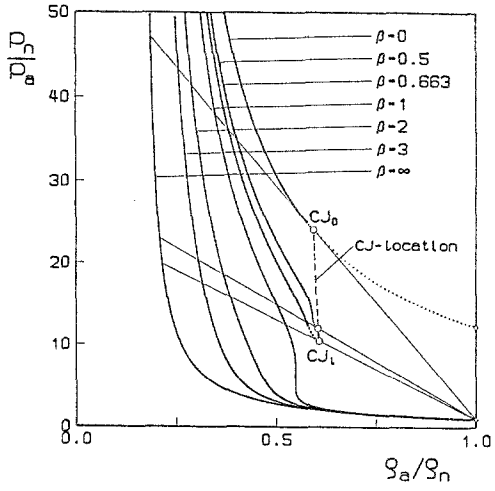

Fig. 3. Rankine-Hugoniot-curves of the reaction fronts and location of the CJ-states

From (64) one may further conclude that for $\beta > 0$ the decay parameters $\lambda_{CJ} > 0$ and varies with the distance ξ. These are the limiting cases of CJ-detonations of variable velocity. In another context, the existence of solutions associated with CJ-detonations of variable velocity was first explored by Oppenheim et al. (1972). Within the scope of a single surface model with the shock wave together with the zone of chemical reactions behind, a CJ-state with variable velocity would be of somewhat paradoxial nature. Therefore, this discrepancy indicates that the reaction zone (front) and leading shock front depart from this point. The possibility of detachment of the detonation wave in the phenomenon of point explosion was first deduced by Korobeinikov (1969), assuming a model with two fronts and a zone of induction.

As a result of the computation with a single surface model it was found that in the regime $0 \leq \beta < 0.664$, where the heat liberated at the wave front is large enough, the spherical shock wave approaches the CJ-state rather quickly. The corresponding CJ-Mach numbers can be called the local CJ-Mach numbers. For a further description it should be possible to use a flow model with two fronts together with the method of characteristics. The introduction of a discontinuity surface at some distance behind the shock wave where the total evolution of heat occurs may probably be incorporated without difficulties (but we must leave that to a coming paper). Here we only give the solution at near surroundings of the uncoupling of the front of an overcompressed detonation wave of variable velocity (cf. Fig. 14). From the point of uncoupling, the shock wave propagates through the unperturbed gas decaying to a sound wave.

In the case when $\beta \geq 0.664$ the reactive blast wave starts to behave more like a nonreacting one ($\beta = \infty$) and never reaches the CJ-state. In this context it is instructive to consider Hugoniot-curves for different values of β plotted in Fig. 3. The plot shows the location of the CJ-states, the Rayleigh-lines, the overcompressed final states and the acoustic point. The dotted continuation of the curve $\beta =$

0 represents a branch of the solution (under compressed detonation), which is not meaningful for problem at hand.

5. Numerical solution

As discussed in our previous paper (Wehle and Gretler 1991), the system of equations (2)–(4) in combination with (7)–(9) is of mixed parabolic-hyperbolic type. Assuming that the heat flux and the heat release are given prior to integration, the system (2)–(4) can be handled as a hyperbolic system and this leads to the following three physical characteristic equations in finite difference form

$$\Delta u^* + \frac{1}{\kappa}\left(\frac{a^*}{p^*}\right)_\eta \Delta p^* = \left[-j\left(\frac{u^* a^*}{r^*}\right)_\eta - (\kappa-1)\left(\frac{a^*}{p^*}\right)_\eta \left(\frac{\partial q^*}{\partial r^*} + j\frac{q^*}{r^*}\right)_\eta\right]\Delta t^*, \quad (65)$$

$$\text{along } \left(\frac{\Delta r^*}{\Delta t^*}\right)_\eta = u^* + a^*,$$

$$\Delta u^* - \frac{1}{\kappa}\left(\frac{a^*}{p^*}\right)_\xi \Delta p^* = \left[j\left(\frac{u^* a^*}{r^*}\right)_\xi + (\kappa-1)\left(\frac{a^*}{p^*}\right)_\xi \left(\frac{\partial q^*}{\partial r^*} + j\frac{q^*}{r^*}\right)_\xi\right]\Delta t^*, \quad (66)$$

$$\text{along } \left(\frac{\Delta r^*}{\Delta t^*}\right)_\xi = u^* - a^*,$$

$$\Delta p^* - \frac{2\kappa}{\kappa-1}\left(\frac{p^*}{a^*}\right)_T \Delta a^* = \kappa\left(\frac{\partial q^*}{\partial r^*} + j\frac{q^*}{r^*}\right)_T \Delta t^*, \quad (67)$$

$$\text{along } \left(\frac{\Delta r^*}{\Delta t^*}\right)_T = u^*,$$

where Δ represents the difference between two adjacent points along a characteristic. The indexes η, ξ and T denote the arithmetic mean values of the coefficients along the right- and left-running characteristics and along the particle path (Fig. 13).

The numerical integration of the system (65)–(67) can be carried out with the technique described in our previous paper (Wehle and Gretler 1991). However in the present case of detonation the numerical integration is performed only for the spherical wave with $\kappa = 1.4$ and with different heat release parameters β. $Q_0 = 20a_a^2$ is used and the perturbation solution for $y = 0.001$ is used as initial condition for the method of characteristics. As stop condition for the iterations an accuracy of 1×10^{-5} was chosen. The number of gridpoints was increased during the computation from 85 to over 300 for a wave propagation Mach number of $M_s = 4.428$. For each increase of gridpoints an adjustement of the point distance Δr^* to the flow state was made according to a stability relation (cf. Wehle and Gretler 1991).

The power expansion and the numerical solution were fitted at a distance of about one percent of the front radius. The dimensionless heat parameter, which describes the heat radiation and heat conduction, was in agreement with (Wehle and Gretler 1991) and (Kailbauer and Gretler 1991), and was chosen to be $\Gamma = 2.5 \times 10^{-4}$.

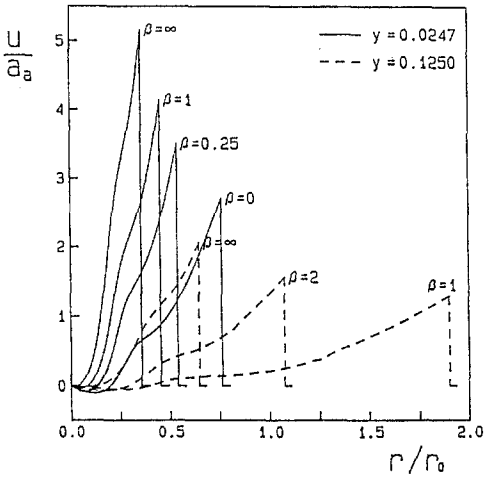

Fig. 4. Non-dimensional velocity as a function of the non-dimensional radius

6. Results

The flow field of a spherical reactive blast wave propagating in a uniform combustible mixture is presented in Figs. 4–7. These show the variation of the non-dimensional particle velocity, pressure, density and sound speed as a function of the non-dimensional radius r/r_0. All the gas-dynamic profiles display typical wave features, they either decay from the explosion wave limit ($\beta = \infty$) to the limit of a CJ-wave ($\beta = 0$) with the propagation Mach number equal to 6.354 ($y_{CJ} = 0.0247$), or to a sound wave (dashed lines) if they have smaller Mach numbers. The decay parameter λ as function of y (Fig. 8) expresses this as the non-dimensional deceleration of the wave front.

It should be mentioned that the numerical calculation breaks down near the CJ-point where the root in (17) goes to zero, but one can observe the exact value of $y_{CJ} = 0.0247$. If the front parameter y is small, the λ-profiles for $0 < \beta \lesssim 2.2$ immediately drop to a minimal value and then, when y grows larger, rise to a maximal value and for $\beta > 2.2$ the curve has an inflection point. Moreover, the graphs show that as the front parameter λ grows larger all the transition curves intersect the curve $\beta = \infty$, which represent the non-reactive wave.

The ratio r_n/r_0 as a function of the front variable y, which is a measure for the propagation Mach number, is illustrated in Fig. 9.

It can be seen from the boundary conditions that the major deviation of the λ-values of the reactive waves from the non-reactive one is caused by the term

$$\frac{Q^*}{W_n^2} = \frac{Q_0^*}{a_a^2} y \exp\left(-\beta\frac{r_n}{r_0}\right), \quad (68)$$

which expresses the heat release at the front. Since this function has two zero points ($y = 0$ and $y = 1$) and a maximum in between, the λ-graph can be completely understood in terms of those influences.

The non-dimensional particle velocity as a function of the non-dimensional distance r/r_0 is depicted in Fig. 4 for two groups, corresponding to two different front parameters $y = 0.0247$ and $y = 0.125$ (dashed lines). One group

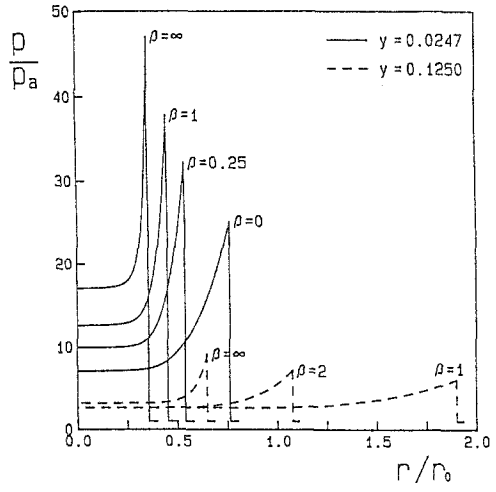

Fig. 5. Non-dimensional pressure as a function of the non-dimensional radius

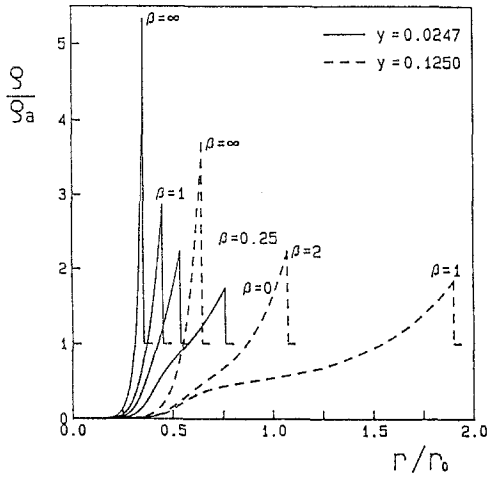

Fig. 6. Non-dimensional density as a function of the non-dimensional radius

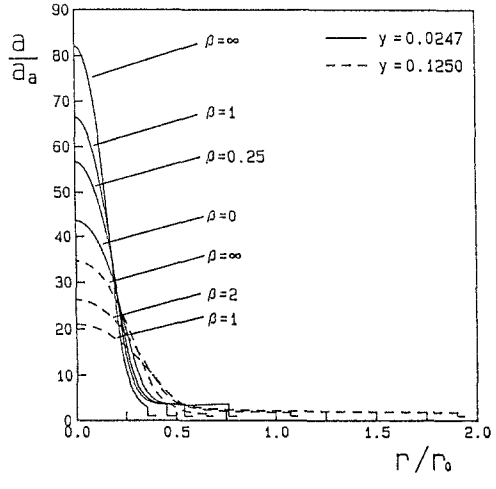

Fig. 7. Non-dimensional speed of sound as a function of the non-dimensional radius

extends between $\beta = \infty$, corresponding to the non-reactive blast wave, and $\beta = 0$, for which the heat released at the wave front is constant and the wave decays to the so-called local CJ-wave with constant front velocity, while the other extends between $\beta = \infty$ and $\beta = 1$ (or $\beta_l = 0.664$) only. There is already at the beginning a negative value of the particle velocity and it only increases very slowly with the radius in this region. The negative velocity in the inner region is generated by cooling of the gas that heat transfer (radiation and conduction) performs. Approximate solutions like those of the quasi-similar method, which is based on the assumption that the logarithmic derivatives of all dependent variables with respect to the front coordinate y are considered constant in the whole flow field, can not describe these backward flow phenomena.

The pressure, that is made non-dimensional by the outer pressure p_a, is shown in Fig. 5 as a function of r/r_0 for two values of the front parameter y and various values of the heat release parameter β. Behind the wave front the pressure decreases rapidly to a nearly constant value in the inner region. On the other hand, it appears that the slope behind the wave front is largest for the non-reactive wave ($\beta = \infty$).

The density distributions for two different front Mach numbers are presented in Fig. 6. If y is small, the density is very small at $r = 0$, and then only increases slowly with increasing radius and increases more rapidly first near the front. The major part of the mass is also concentrated to the front. At later times this changes and an inflexion point occurs, which approaches the center with time. The radius becomes larger for smaller β, which indicates the same effect due to the heat release as mentioned above.

In Fig. 7 the sound speed, from which one can determine the temperature with the relation $T/T_a = a^2/a_a^2$, is presented as a function of the radius. The sound speed has its maximum at the center and decreases with increasing radius to the value at the wave front. With decreasing propagation Mach number and heat release coefficient β the sound speed is reduced and therefore also the temperature in the whole flow field. At large times the sound speed has taken the value of the undisturbed gas, with the inner region excepted (see also our previous paper Wehle and Gretler 1991).

Figures 10–12 show the dependence of the non-dimensional density, particle velocity, and pressure as a function of the ratio r_n/r_0 for $\beta = 0$, 0.5, 0.663, 1, 2, 3 and ∞. The dashed lines represent the local CJ-limit of constant propagation velocity or variable propagation velocity where uncoupling of the overcompressed detonation waves occurs. Comparing the transition waves at the same distance from the center it can be said that the peak pressure is largest for the CJ-wave, where the chemical energy is constant. Exactly the opposite is the case if we compare the transition curves of the density at a constant distance from the explosion center, as shown in Fig. 10.

Another way to illustrate the characteristics of detonation waves is, as in Fig. 10, with the variation of the peak density ratio on the wave front as a function of the distance r_n/r_0 for $\beta = 0$, 0.5, 0.663, 1, 2, 3 and ∞. In the early stage, i.e. for small r_n/r_0, the peak value for small β (large chemical

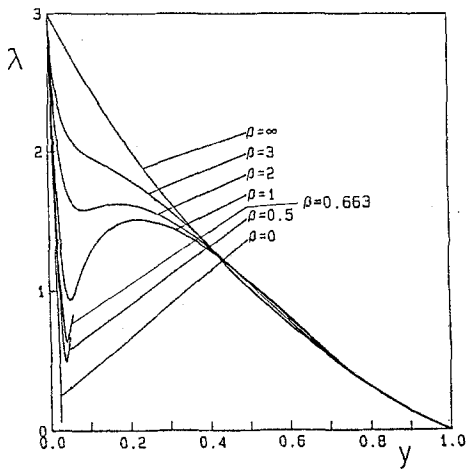

Fig. 8. Non-dimensional deceleration of the wave front as a function of the reciprocal square of the reaction front Mach number $y = (a_a/W_n(t))^2$

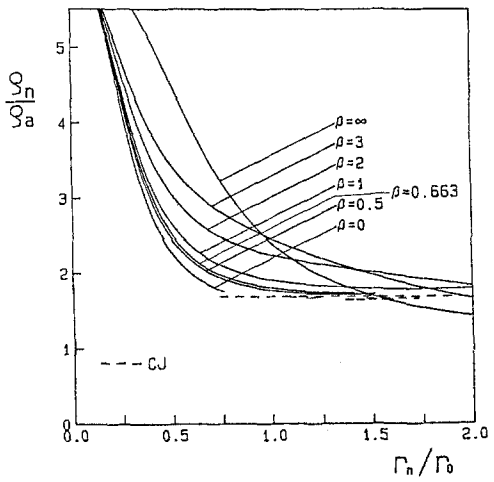

Fig. 10. Non-dimensional density at the reaction front as a function of the non-dimensional front radius

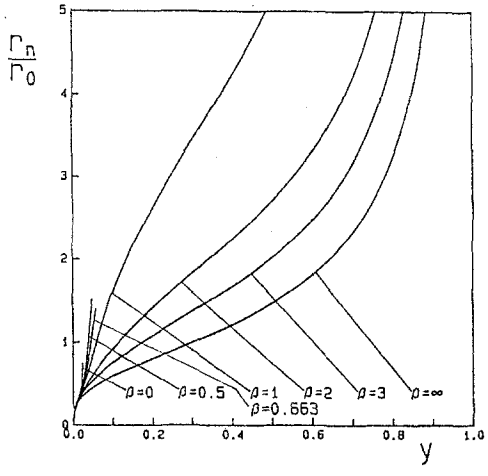

Fig. 9. Non-dimensional front radius r_n/r_0 as a function of the reciprocal square of the reaction front Mach number $y = (a_a/W_n(t))^2$

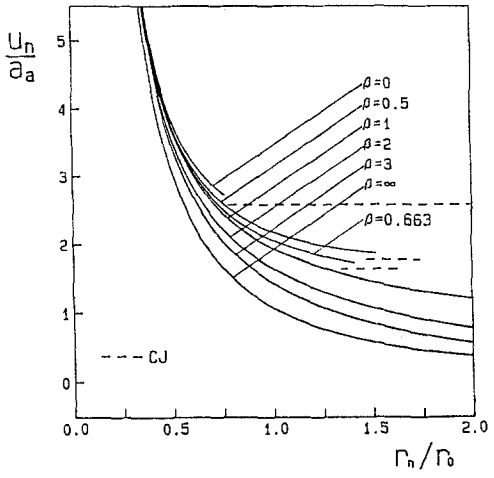

Fig. 11. Non-dimensional velocity at the reaction front as a function of the non-dimensional front radius

energy) is smaller than that for large β (small chemical energy).

From Fig. 9, for example, it follows that for the same value y or Mach number M_n the distance r_n/r_0 is larger for detonation waves than for the explosion wave, but Fig. 10–12 then indicate that the peak values for large β are larger than for small β. Moreover, the peak densities for $\beta < 0.664$ approach to the CJ-limit value (dashed lines in Fig. 10).

Chemical heating from the detonation increases the velocity at the front but reduces or increases slightly the density in the near field or far field solution, respectively.

Figure 13 shows the plane of the physical characteristics for $\beta = 0$. The end points of the curves correspond to the transition to the CJ-regime. We remark also that at the center of explosion the slope of the physical characteristics have finite values due to the influence of internal heat conduction and thermal radiation.

Finally, Fig. 14 shows the dependence of the law of motion of an overcompressed spherical detonation wave on time $r_n(t)$ in the cases $\beta = 0$, 0.5, and 0.663. The end point $\beta = 0$ corresponds to the limiting case of constant heat release with transition to the CJ-detonation wave of constant velocity. However, in the case of variable heat release, the end points $\beta = 0.5$ and 0.663 correspond to the above-noted detachment of the detonation waves and can be identified with the so-called local CJ-states of variable velocities.

7. Conclusions

The results of numerical calculations reveal the following significant facts:

(1) The physical quantities such as velocity, density, pressure and temperature are strongly influenced by the heat release function.

(2) A reacting blast wave decriebed by a single front model decays either to a sound wave or to the local CJ-wave.

(3) Detonation waves reach the local CJ-state only if the heat liberated at the wave front is large enough, which

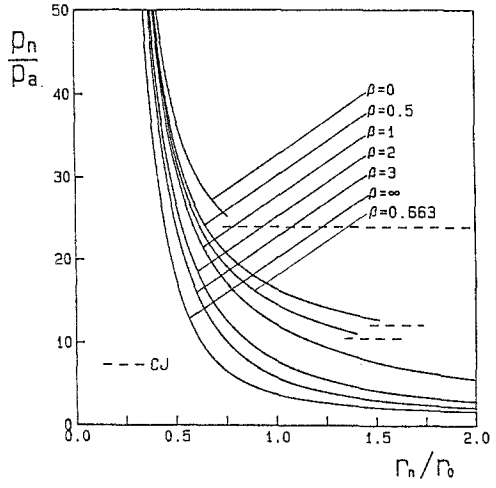

Fig. 12. Non-dimensional pressure at the reaction front as a function of the non-dimensional front radius

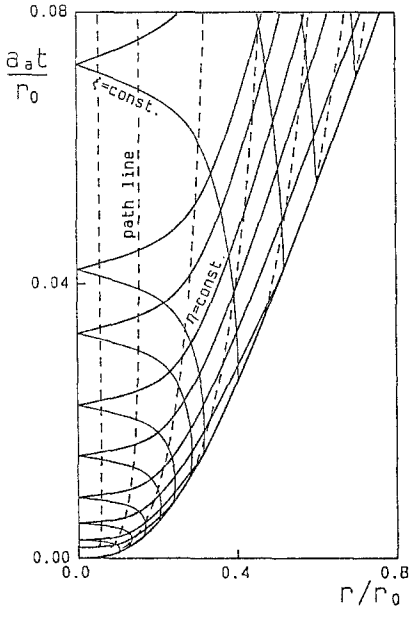

Fig. 13. Physical plane of a detonation wave in the single front model for $\beta = 0$

requires that $0 \leq \beta < 0.664$. For $\beta \geq 0.664$ the reactive blast waves start to behave more like a non-reactive one.

(4) For $0 < \beta < 0.664$ the single front model loses its validity at the local CJ-state (uncoupling point of shock front and reaction front). For further description of the problem a two front model should be used.

(5) Including the thermal radiation and heat conduction remedies the basic flaw in the classical blast wave theory by yielding non-zero density and consequently finite temperature at the center of symmetry.

(6) In contrast to Oshima's quasi-similarity approximation, using the present method the density profiles satisfy the mass integral and finally, the velocity profiles are accurate around the center of symmetry since in this region the particle velocity is negative as expected.

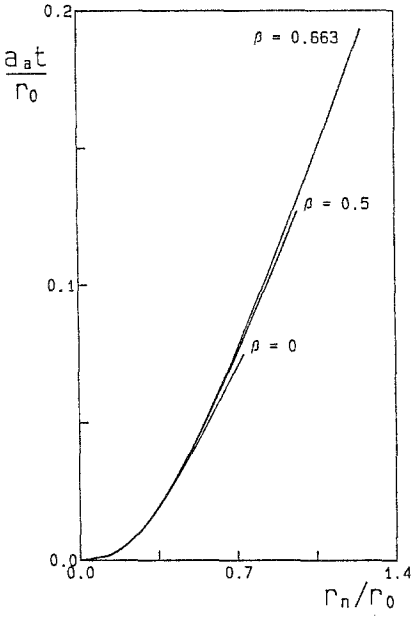

Fig. 14. Non-dimensional front radius r_n/r_0 as a function of the non-dimensional time $a_a t/r_0$

Nomenclature

Latin symbols

a speed of sound
e specific internal energy
E_i explosion energy
E_j blast wave energy
f nondimensional particle velocity
g nondimensional pressure
h nondimensional density
I mass integral
j factor of symmetry
J energy integral
K thermal conductivity
K_a constant
M_j blast wave mass
M_s shock Mach number
n_j geometrical factor
p pressure
q total heat flux
q_C heat flux by conduction
q_R heat flux by radiation
Q chemical heat release
Q_0 constant
r space coordinate
r_0 characteristic length of flow field
t time coordinate
T absolute temperature
u particle velocity
W_n front propagation velocity
x similarity variable
y front variable

Greek symbols

α_R Rosseland mean absorption coefficient
α_{R_a} constant
β_C temperature exponent of thermal conductivity
β_R temperature exponent of absorption coefficient
Γ nondimensional heat flux parameter
Γ_C conduction parameter
Γ_R radiation parameter
Δ finite difference
κ specific heat ratio
λ decay parameter
ξ nondimensional shock radius
π ratio between perimeter and diameter of a circle
ρ density
σ Stefan-Boltzmann constant

Subscripts

0, 1 zeroth, first order
a undisturbed gas
CJ Chapman-Jouguet
i condition at the center
n conditions immediately behind the shock front
T particle path
η along characteristic $\eta = const.$
ξ along characteristic $\xi = const.$
$*$, $\sim$ nondimensional variable
$\dot{}$, $\ddot{}$ differentiation with respect to time
$'$ differentiation with respect to x

References

Abdel-Raouf AM, Gretler W (1991) Quasi-similar solutions for blast waves with internal heat transfer effects. Fluid Dynamics Research 8:273–285

Jouguet E (1917) In: Doin et fils (ed) La mechanique des explosifs. Paris, pp 359–366

Kailbauer F, Gretler W (1991) Perturbation solutions for blast waves with convective and radiative heat transfer. Acta Mechanica 88:127–140

Korobeinikov VP (1969) The problem of point explosion in a detonating gas. Astronautica Acta 14:411–419

Ohyagi S, Ohsawa A (1983) Analysis of reactive blast waves propagating through gaseous mixtures with spatially distributed chemical energy. In: Bowen JR, Manson N, Oppenheim AK, Soloukhin RI (eds) Shock waves, explosions and detonations (Progress in astronautics and aeronautics 87). pp 157–174

Oppenheim AK, Kuhl AL, Kamel MM (1972) On self-similar blast waves headed by the Chapman-Jouguet detonation. J Fluid Mech 55:257–270

Oppenheim AK, Lundstrom EA, Kuhl AL, Kamel MM (1971) A systematic exposition of the conservation equations for blast waves. Journal of Applied Mechanics 38:783–794

Oshima K (1960) Quasi-similar solutions of blast waves. Aero Research Institute, Report No. 386, University of Tokyo

Pomraning GC (1973) The equations of radiation hydrodynamics. In: Ter Haar D (ed) Int Ser Monographs in Natural Philosophy 54. Pergamon Press, Oxford, pp 88,91–92

Taylor GI (1950) The dynamics of the combustion products behind plane and spherical detonation fronts in explosives. Proc R Soc A 200:235–247

Wehle P, Gretler W (1991) Numerisches Charakteristikenverfahren zur Berechnung der Explosion. Acta Astronautica 25:209–221

Zel'dovich Y (1942) Distribution of pressure and velocity in the products of a detonating explosion, and in particular in the case of a spherical propagation of the detonation waves. Journal of Exp Theor Phys (USSR) 12:389–406

This article was processed using Springer-Verlag TEX Shock Waves macro package 1.0 and the AMS fonts, developed by the American Mathematical Society.